Direct solar energy-mediated synthesis of tertiary benzylic alcohols using a metal-free heterogeneous photocatalyst

Direct Solar Energy Mediated Synthesis of Tertiary Benzylic Alcohols Using A Metal-Free Heterogeneous Photocatalyst

Yu Zhang,[a,b,†] Shaowei Qin,[a,†] Nathalie Claes,[c] Waldemar Schilling,[a] Prakash Kumar Sahoo,[b] H. Y. Vincent Ching,[b] Aleksander Jarowski,[e] Filip Lamiere,[f] Adam Slabon,[e] Sabine van Doorslaer,[d] Sara Bals,[c] Shoubhik Das[b*]

a. Institut für Organische und Biomolekulare Chemie, Georg-August-Universität Göttingen, Tammannstraße 2, 37077 Göttingen, Germany

b. ORSY Division, Department of Chemistry, University of Antwerp, Groenenborgerlaan 171, 2020 Antwerp, Belgium .

c. EMAT, University of Antwerp, Groenenborgerlaan 171, 2020 Antwerp, Belgium.

d. BIMEF, Department of Chemistry, University of Antwerp, Universiteitsplein 1, 2610 Antwerp, Belgium.

e. Department of Materials and Environmental Chemistry, Stockholm University, 10691 Stockholm, Sweden.

f. BAMS, Department of Chemistry, University of Antwerp, Groenenborgerlaan 171, 2020 Antwerp, Belgium.

E-mail: Shoubhik.Das@uantwerpen.be

ABSTRACT

Direct hydroxylation *via* the functionalization of tertiary benzylic C(sp^3)-H bond is of great significance for obtaining tertiary alcohols which find wide applications in pharmaceuticals as well as in fine chemical industries. However, current synthetic procedures use toxic reagents and therefore, the development of a sustainable strategy for the synthesis of tertiary benzyl alcohols is highly desirable. To solve this problem, herein, we report a metal-free heterogeneous photocatalyst to synthesize the hydroxylated products using oxygen as the key reagent. Various benzylic substrates were employed into our mild reaction conditions to afford the desirable products in good to excellent yields. More importantly, gram-scale reaction was achieved *via* harvesting direct solar energy and exhibited high quantity of the product. The high stability of the catalyst was proved *via* recycling the catalyst and spectroscopic analyses. Finally, a possible mechanism was proposed based on the EPR and other experimental evidence.

INTRODUCTION

Oxygenation reactions are fundamentally important not only in nature but also in academia as well as in industrial research. A large number of oxygen-containing drugs and natural products have been used as antibiotics, anticoagulants, nutrients, cosmetics, etc., and play vital roles in our daily life.[1-3] Among the oxygenated products, tertiary alcohols are valuable compounds which can be used as intermediates for various coupling reactions as well as pharmaceutical drugs (**Scheme 1a**).[4-6] Therefore, introducing a hydroxy group directly *via* the functionalization of C–H bond is one of the attractive research topics. Additionally, it is worth to mention that the tertiary benzyl alcohols are always expensive compared to the corresponding staring materials. For example, the price of 4-bromocumene is 8.6 €/g, but the price of the corresponding hydroxylated product is *ca* 105.0 €/g (TCI Europe). This price comparison directly suggests the strong importance for the hydroxylation reactions via the functionalization of tertiary C−H bond.

To date, tremendous efforts for the C(sp^3)−H hydroxylation reaction have been made to achieve hydroxylated products using transition-metal catalysis, enzyme catalysis, electrocatalysis etc.[7-19] In 2004, Lykakis and co-workers have reported photo-oxidation of the *para*-substituted cumene in the presence of O_2 and Et_3SiH with W-based catalyst.[16] With the addition of Et_3SiH, the cumyl peroxyl radical was trapped, thus, the possibilities for the decomposition to the corresponding aryl ketone or the associated rearrangement to the corresponding cumyl radical was suppressed. In 2017, the Chen group described a photocatalytic strategy for benzylic C−H hydroxylation reaction using hypervalent iodine as an oxidant and a HAT reagent to facilitate the generation of tertiary or benzylic radicals. Radicals were further oxidized by the photocatalyst to form the radical cations, followed by the trapping of nucleophiles, provided the desired products.[17] Later, the Ritter group reported an alternative for the construction of benzylic mesylates, which can easily be converted to benzylic alcohols.[18] Notably, it showed a good site selectivity at the benzylic C(sp^3)−H bond in the presence of other C(sp^2)−H bonds,

which was attributed to the generation of benzyl radical via a proton coupled electron transfer (PCET) pathway. A new general trifluoromethylated dioxirane-mediated C(sp^3)−H oxidation reaction through a continuous flow process has been reported recently. This method employed inexpensive reagents and was applied to various substrates bearing a large range of functionalities (**Scheme 1b**).[19]

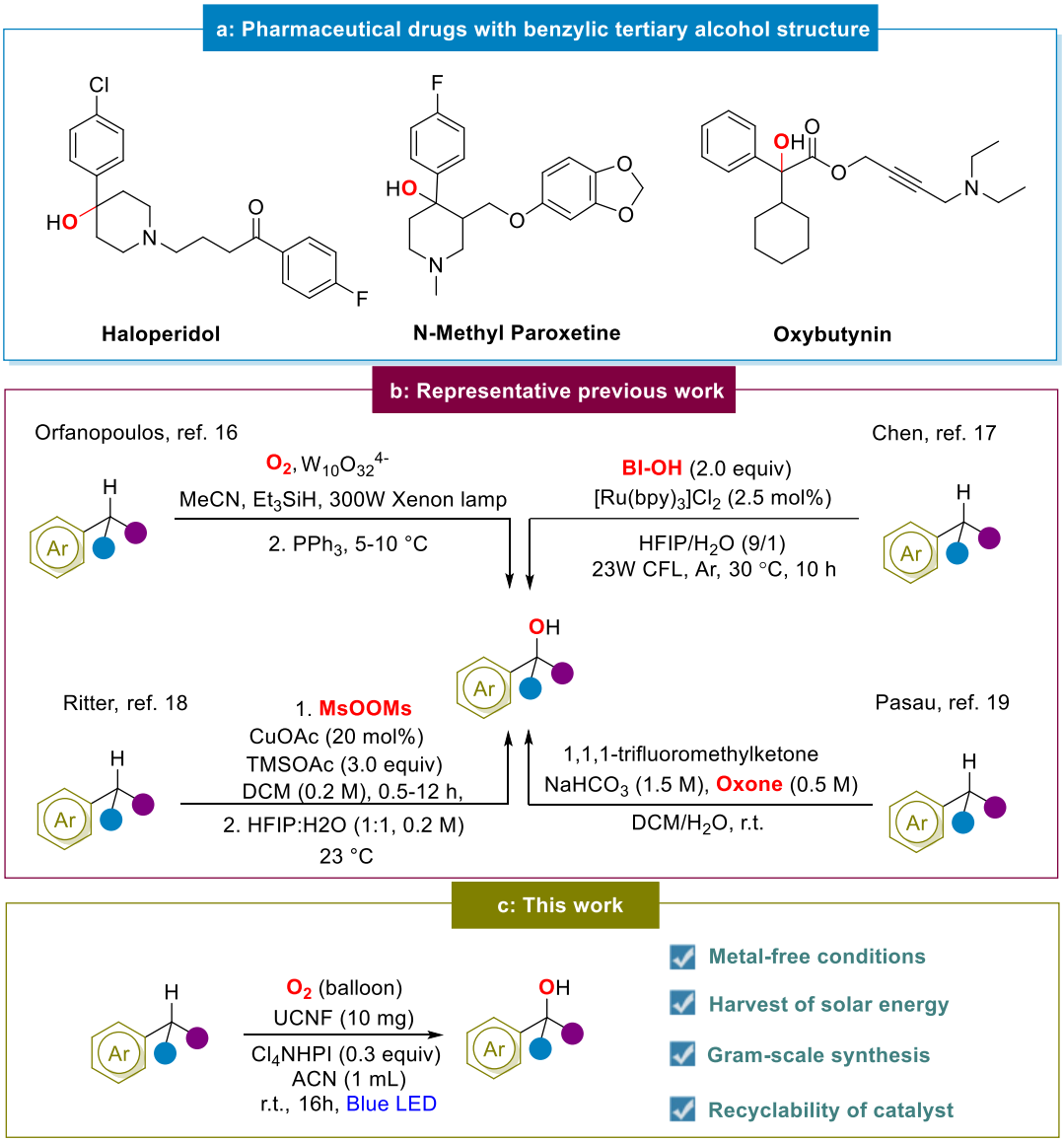

Scheme 1. Overview of the hydroxylation of benzylic C(sp^3)-H bond. a. Pharmaceutical drugs with benzylic tertiary alcohol motifs; b. Previous reports of benzylic C(sp^3)-H hydroxylation; c. This work.

To the best of our knowledge, the tertiary benzylic C(sp^3)−H hydroxylation utilizing metal-free photocatalyst has never been reported. In general metal-free systems are highly attractive since it avoids high-cost and toxic reagents, and significantly lowers the carbon-footprint of the whole process.[20-23] Additionally, it's a challenging direction in organic synthesis and an interesting avenue for the pharmaceutical sector.[24] More importantly, due to the industrial indispensability, heterogeneous catalysts serve as a topic of great interest in both the experimental and theoretical studies.[25,26] It should be noted that from the sustainability perspective, nitrogen-substituted carbon and polymeric carbon nitrides (PCN) are potential green photocatalysts, due to their design based on abundant elements.[27,28] Since the pioneering work of *Antonietti* et *al.* on C_3N_4 catalysts in 2009, metal-free semiconductors have been emerged as powerful photocatalysts for water splitting and expanded towards more complex chemical reactions.[29-31] Despite a safe and relatively easy synthesis, the elucidation of structure-property relationship

in PCN remains still challenging when it comes to understand the catalytic mechanisms on the atomic level. For instance, nitrogen-deficiency has been considered to play a decisive role in the photocatalytic performance.[32] Given the difference in one electron between carbon and nitrogen, structure determination *via* diffraction is limited. Nevertheless, solid state nuclear magnetic resonance (NMR) spectroscopy is a powerful tool, but usually require expensive ^{15}N labelling. We recently demonstrated that ^{15}N solid state NMR spectroscopy is a powerful even at natural ^{15}N abundance to determine the nitrogen positions in N-doped carbon materials.[24,33] Based on this research work, a metal-free polymeric photocatalyst in the form of semiconducting carbon nitride (PCN)/*N*-Hydroxy tetrachlorophthalimide (Cl_4NHPI) catalytic system has been presented which afforded highly-valuable hydroxylated products. In this case, the PCN activated the molecular oxygen, which played a key role as the oxygen source and reacted with Cl_4NHPI to afford Cl_4PINO radical as a hydrogen atom transfer (HAT) reagent **(Scheme 1c).** The stability of the catalyst was proved by recycling the photocatalyst at least five times and by detailed spectroscopic analyses.

EXPERIMENTAL SECTION

Standard Reaction Procedures.

Hydroxylation reactions were carried out under water-free conditions and oxygen atmosphere (balloon). For this purpose, the reaction flask and stirring bar were dried in an oven over four hours to remove the moisture. Afterwards, to the dried two necked flask (with stirring bar), a mixture of 0.3 mmol (1.0 equiv.) substrates, 10 mg of polymer carbon nitride (PCN), and 27 mg of Cl_4NHPI (0.3 equiv.) was added subsequently. Then the flask was evacuated and flushed with nitrogen (2 x) and oxygen (1 x) via Schlenk techniques. Dry acetonitrile (1.0 mL) as a solvent was transferred with a nitrogen-flushed (3 x) syringe through a rubber septum into the reaction flask. The reaction mixture was stirred at room temperature under the irradiation of blue LED (16 W) for 16-48 h. The reactions were monitored by TLC and GC-MS. The reactions were quenched with 10 mL of distilled water and 10 mL of ethyl acetate. The combined organic layers were extracted with ethyl acetate and concentrated in vacuo, then purified via flash column chromatography. GC-MS, ^1H NMR, and $^{13}C\{^1H\}$ NMR were employed to characterize the products.

General Procedure for the Hydroxylation using Sunlight

A 50-mL two-necked flask containing a stirring bar was charged with 1.0 g of substrate, 80 mg of PCN and 30 mol% of Cl_4NHPI. After evacuating the flask three times and purging it two times with nitrogen, oxygen atmosphere was incorporated through an O_2 balloon. Finally, dry acetonitrile (10.0 mL) was added. The resulting mixture was stirred under sunlight and the progress was monitored *via* GC-MS. Then, the resulting mixture was subjected to an aqueous workup (using distilled water; or brine in case of slurry phase separation) and was extracted three times with ethyl acetate. The combined organic layers were dried over anhydrous Na_2SO_4, filtered and concentrated *in vacuo*. Products were purified *via* silica gel chromatography with ethyl acetate and *n*-hexane as solvents. GC-MS, ^1H NMR, and $^{13}C\{^1H\}$ NMR were employed to characterize the products.

General Procedure for the spectroscopic measurement of the catalyst.

The morphology of the catalyst materials was investigated by scanning electron microscopy (SEM). The catalyst powder was deposited on carbon tape, the SEM was operated at 15 kV and secondary electrons were used for imaging. In order to evaluate the crystallinity of the sample and its morphology in more detail, transmission electron microscopy (TEM) was performed. The catalyst powder was crushed in ethanol and deposited on a TEM grid. The catalyst materials were characterized by bright field TEM (BF-TEM) and high angle annular dark field scanning transmission electron microscopy (HAADF-STEM) using a Tecnai Osiris microscope (Thermo Fischer Scientific) operated at 200 kV. To determine the elemental composition, energy dispersive X-ray spectroscopy (EDX) measurements were carried out

using a ChemiSTEM system (Super X detector) and analyzed using the Bruker ESPRIT software.

Electron paramagnetic resonance (EPR) studies

Room temperature continuous wave (cw) X-band EPR measurements were carried out on a Bruker Elexsys E680 spectrometer mounted with an optically accessible ER4104OR resonator working at ~ 9.44 GHz. The spectra were collected 1 mW microwave power, 0.05 mT modulation amplitude and 100 kHz modulation frequency. A diode 447 nm laser operating at ~ 100 mW was used for illumination experiments. The EPR spectra were simulated with Matlab2018b using the EasySpin-6.0 module.

RESULTS AND DISCUSSION

At the outset, we have synthesized a polymeric carbon nitride (PCN) according to a literature report.[32] The optical bandgap of the PCN (2.39 eV) was determined by tauc plot (**Figure S3**), the conduction band (CB) was measured by Mott-Schottky experiments and the ECB was estimated to be ca. -0.91 V vs. RHE. Brunauer–Emmett–Teller specific surface area (SBET) was determined from the low-temperature nitrogen adsorption/desorption isotherms and found to be 37 $m^2 \cdot g^{-1}$ for the catalyst (**Figure S4, S5)**. It was further applied for the investigations of hydroxylation reaction of benzylic C(sp^3)-H bonds. We started to optimize the reaction conditions using cumene (**1a**) as the model substrate. The results of the screening and optimizations are shown in **Table 1**. A limited yield of the product was found using the heterogeneous catalyst without any HAT reagents (**Entry 1**). Afterwards, a HAT reagent (Cl_4NHPI) was added into reaction conditions, to our delight, the yield was improved to 65%. In this case, Cl_4NHPI was proposed to give an oxyl radical which abstracted a hydrogen atom from the substrate. Thereby, a benzylic radical was generated via HAT pathway. However, adding higher amount of the catalyst could not further improve the yield (**Entries 2–4)**. Moreover, different solvents were investigated but could not further improve the yield of the reaction (**Entries 5–7)**. Notably, only the HAT reagent itself without the presence of the catalyst also provided the product but in limited yield (**Entry 8**). It is supposed that the initiation of Cl_4PINO (PINO = phthalimide *N*-oxyl) radical is the key step,[34] without co-catalyst for Cl_4NHPI activation, Cl_4PINO radicals was only generated slowly under the irradiation of blue-LED. Cooperation with the catalyst, accelerated this step and generated enough Cl_4PINO radical in the reaction. The further control experiments clearly proved the indispensable role of the light and oxygen in this reaction (**Entries 9–10)**.

Table 1. Optimization studies for the synthesis of 2-phenyl-2-propanol (**1b**).[a-b]

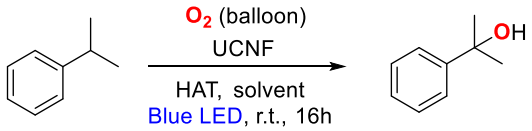

1a **1b**

Entry	UCNF	Cl_4NHPI	Solvents	T (h)	Light	Atmos-phere	Yield (%)[b]
1	10 mg	0 eq.	MeCN	16	on	O_2	23
2	**10 mg**	**0.3 eq.**	**MeCN**	**16**	**on**	**O_2**	**65**
3	12 mg	0.3 eq.	MeCN	16	on	O_2	65
4	15 mg	0.3 eq.	MeCN	16	on	O_2	63
5	10 mg	0.3 eq.	THF	16	on	O_2	15
6	10 mg	0.3 eq.	DMSO	16	on	O_2	9

7	10 mg	0.3 eq.	DMF	16	on	O_2	24
8	0 mg	0.3 eq.	MeCN	16	on	O_2	16
9	10 mg	0.3 eq.	MeCN	16	off	O_2	0
10	10 mg	0.3 eq.	MeCN	16	on	N_2	1

[a] General reaction conditions: oxygen, 12 W blue LED, 0.3 mmol **1a** (1.0 eq.), 0.3 eq. of Cl_4NHPI, 10 mg of photocatalyst, 1 mL solvent, room temperature, 16 h. [b] Yields were determined by GC using dodecane as an internal standard.

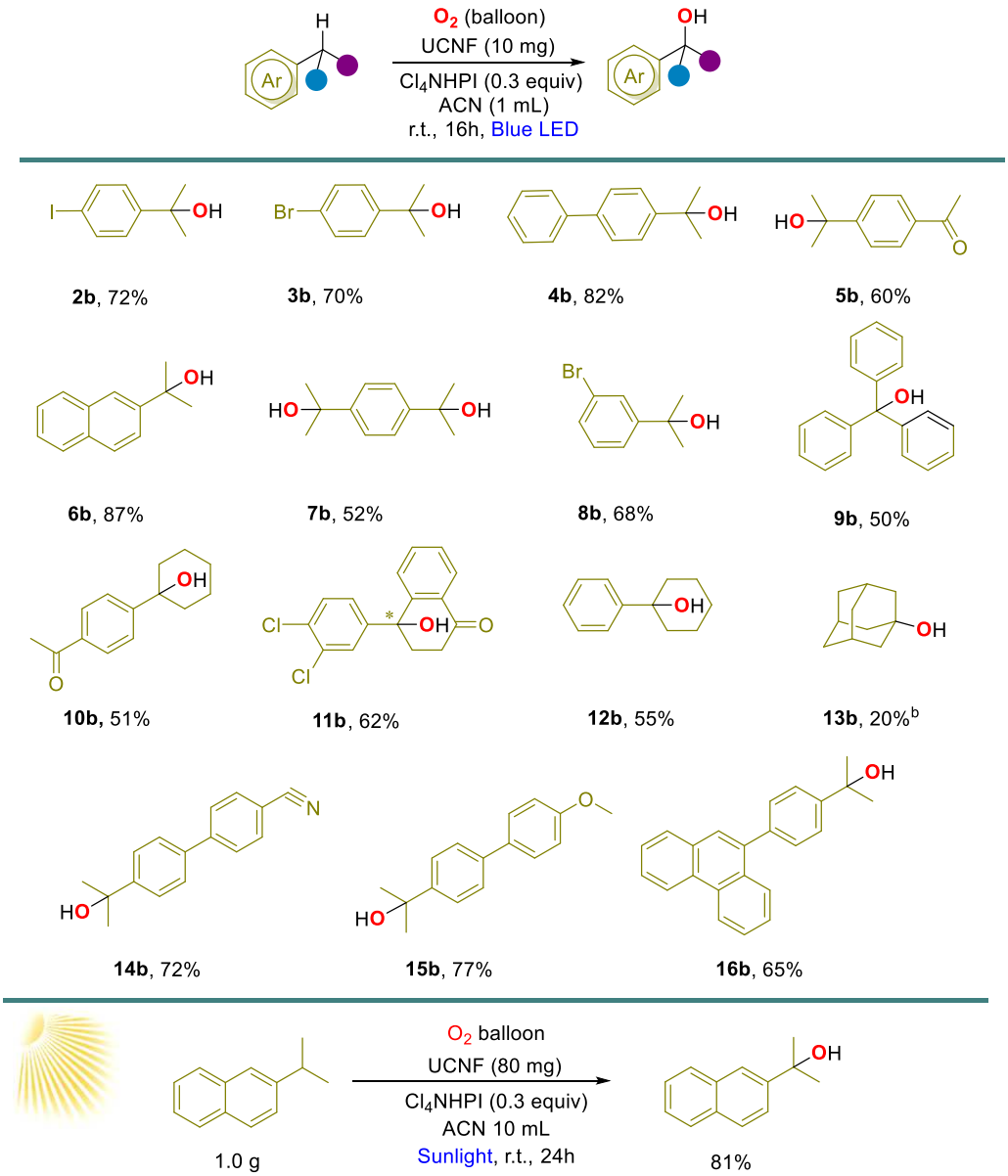

Scheme 2. Substrate scope of photocatalytic hydroxylation. [a] Reaction conditions: O_2 (balloon), 12 W blue LED, 0.3 mmol substrate, 10 mg catalyst, 0.3 eq. Cl_4NHPI, 1 mL ACN, 16h–48 h. [b] The yield was determined by GC with dodecane as an internal standard.

With the best reaction conditions in the hand, various substrates were employed to afford the corresponding hydroxylated products. As shown in **Scheme 2**, the scope was firstly extended to substituted isopropyl benzenes such as 4-iodoisopropylbenzene, 4-bromoisopropylbenzene and 4-isopropylbiphenyl (**2b–8b**). To our delight, all of them exhibited good reactivity under the standard conditions in good to excellent yields. Furthermore, we also applied these mild reaction conditions to triphenylmethane which also formed the corresponding hydroxylated

product with medium isolated yield probably due to the steric hindrance of the triphenyl structure (**9b**). It should be noted that those hydroxylated products, such as **5b** (770 $/g, CAS No. 54549-72-3, Ambeed), are highly expensive chemicals. The scope was further extended to other substrates having benzylic C(sp^3)-H bonds including phenylcyclohexane and 4'-cyclohexylacetophenone (**10b–12b**) under these reaction conditions. Adamantane (**13b**) was also employed in our reaction conditions, which showed limited reactivity under our system. To extend the substrate scope, more isopropyl benzenes (**14b–16b**) were applied to the chosen conditions to afford desirable hydroxylated products in good yields. Afterwards, we aimed to replace the blue LEDs by harvesting direct sunlight and even for the gram scale reaction. To our delight, 2-isopropyl naphthalene (**6b**) was highly compatible with an excellent isolated yield of the desired product. Considering the high value of tertiary alcohols in chemical industries, this metal-free semi-heterogeneous catalytic system will certainly provide a direct methodology to construct tertiary alcohols.

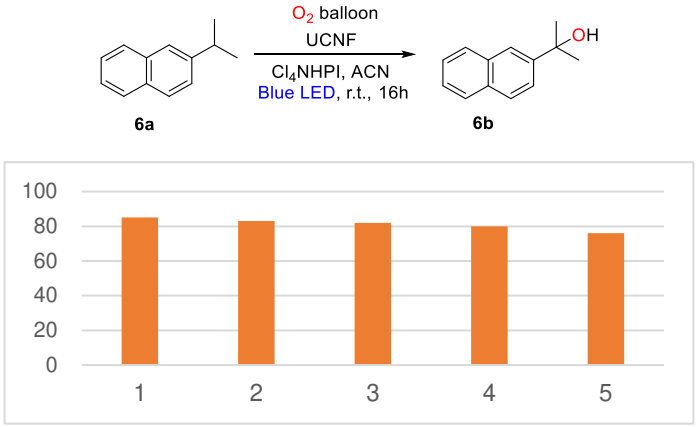

Scheme 3. Reusability of PCN for hydroxylation of 2-isopropylnaphthalene.

To ensure the stability of the catalyst, experiments with a recycled catalyst were performed at least 5 times under the same reaction conditions and to our delight, this catalyst was recycled with stable reactivity (**Scheme 3**). The detailed procedure of recycling the catalyst is given in the experimental section (**See the SI, section 4**). To further investigate the stability of the catalyst, freshly prepared and recycled catalysts were investigated by the electron microscopy. The morphology was investigated by SEM and STEM imaging (**Figure 1**, a-b, d-e). Similar structures were observed in the fresh and recycled catalysts. Moreover, HRTEM images and the corresponding Fast Fourier Transform demonstrated the amorphous nature of both the catalysts (**Figure 1**, **2**). In addition, the elemental composition was investigated by EDX measurements. For the freshly prepared catalyst, the Cliff-Lorimer quantification of the EDX spectra showed the presence of on average C (55.1 ± 1.9) wt%, N (43.8 ± 1.5) wt% and O (1.2 ± 0.1) wt% based on 6 measurements. For the recycled catalyst, the presence of on average C (55.5 ± 1.9) wt%, N(43.6 ± 1.5) wt% and O (1.0 ± 0.1) wt% was also observed. This showed that the elemental composition has not changed during catalysis and after recycling the catalyst material.

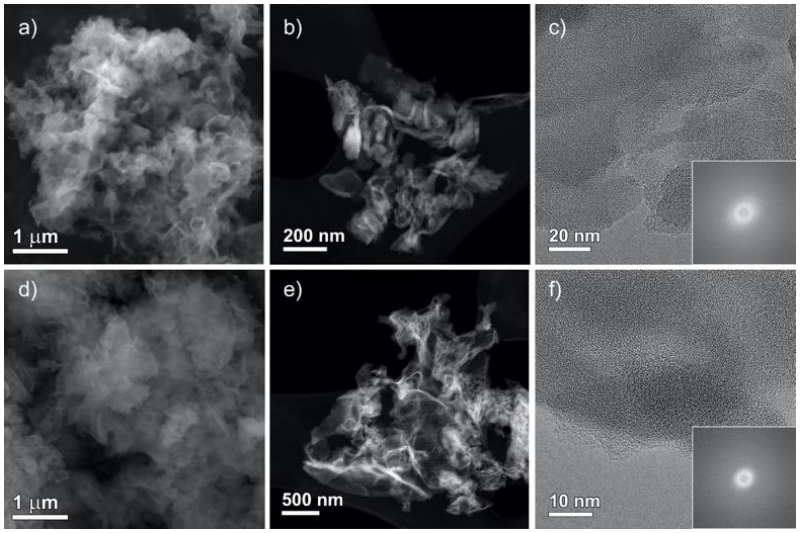

Figure 1. SEM (a,d), HAADF-STEM (b,e) and HRTEM (c, f) images of the freshly prepared (a-c) and recycled (d-f) catalyst. The inset in figures c and f is the calculated Fast Fourier Transform of the region, showing the amorphous nature of the catalyst materials.

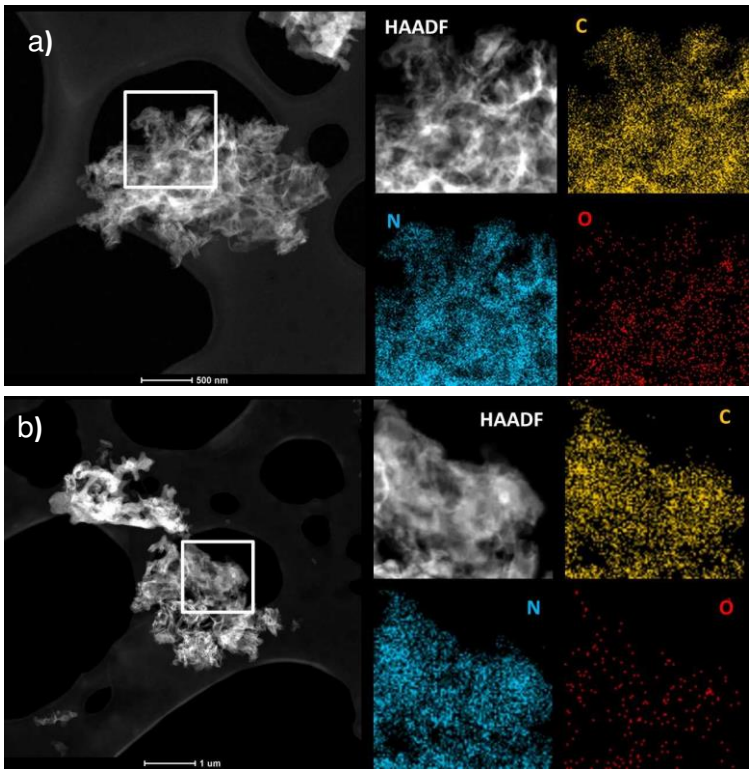

Figure 2. EDX spectra of the (a) fresh and (b) recycled catalyst show the presence of C, N and O. Cu is present from the supporting grid and holder.

To shed light on the details of the catalyst, the solid-state NMR spectra of the PCN was presented together with the model structure of melem monomer unit (**Figure 3**). Proton spectrum (panel a) revealed two main signals: that from NH linkers at 9.0 ppm and that from NH_2 terminal groups at 4.1 ppm. The high intensity of the signal from NH linkers compared to that of NH_2 terminal groups (roughly ~6:1) indicated a highly condensed/polymerized network. The two observed ^{13}C resonances (panel b) originated from the "edge" (C_e; 165 ppm shift) and the "internal" (C_i; 156 ppm) carbon sites, as marked on the structural model in panel d. The signal of C_e was expected to have higher intensity than that from C_i as a consequence of closer distances to protons of the NH and NH_2 groups, which in turn allowed for more efficient cross-polarization in the CPMAS experiment. No other carbon signals from aromatic or non-aromatic

species were observed in the ^{1}H-^{13}C CPMAS spectrum. In the ^{1}H-^{15}N CPMAS spectrum all nitrogen resonances expected for the PCN structure composed of melem monomer units were discernible. Signals at -188 and -220 ppm were correspond to the nitrogen atoms situated at the edge (N_e) and inside (N_i) of the monomer units, respectively. The N_e/N_i signal intensity ratio was higher than the expected 6:1, because N_i sites experienced further distances to the closest protons, which made cross-polarization less efficient for this nitrogen site. The intensities of both these signals increased when the contact time in CPMAS experiment was increased from 2 to 4 ms, which corroborated signal assignments. Resonances at -243 and -264 ppm originated from the linkers (NH) and terminal NH_2 groups, respectively. Note that the intensity of the signal of the NH_2 groups was overrepresented in the ^{1}H-^{15}N CPMAS spectrum since there were two available protons to cross-polarize from compared to the NH moiety. These signal assignments were in pair with previous NMR study on $^{13}C/^{15}N$-isotope enriched PCN,[35] and with theoretical predictions of $^{13}C/^{15}N$ NMR shifts in PCN by DFT.[36] It should be noted that the ^{1}H-^{13}C (b), and ^{1}H-^{15}N CPMAS (c) spectra of PCN resemble recently reported patterns of polymeric carbon nitrides with aryl amino groups despite a significantly smaller surface area.[24] This result indicates that the structure of C_3N_4-derived polymeric units is relatively independent of the corresponding surface area, i.e. the role of nitrogen defects may have been overestimated in previous reports with respect to photocatalytic activity.

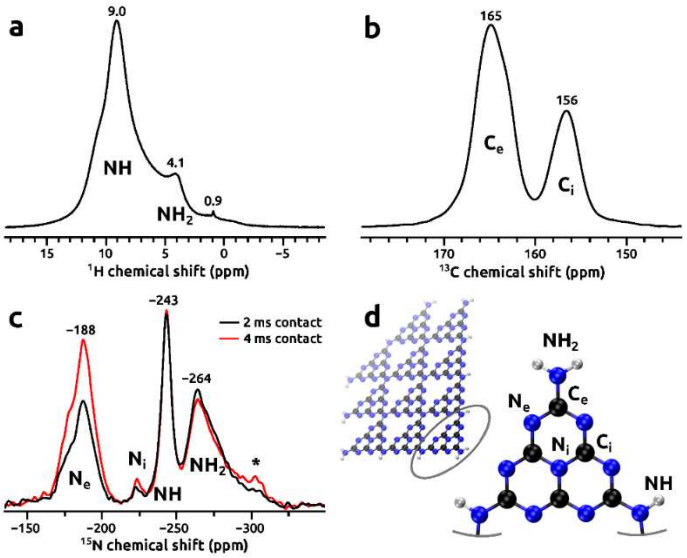

Figure 3: ^{1}H MAS NMR (a), ^{1}H- ^{13}C (b), and ^{1}H- ^{15}N CPMAS (c) spectra of PCN collected at 14.1 T. The ^{1}H- ^{15}N CPMAS spectrum shown for two contact intervals: 2 and 4 ms; spinning sideband marked with an asterisk. Structural fragment (d) displays the NMR signals assignments.

After achieving the characterization information, the ^{18}O-labeling experiment was performed with $^{18}O_2$ (Sigma Aldrich, ^{18}O atom 99.7%), and was analyzed with ESI-HRMS and NMR which showed the ^{18}O-labeled product with an isolated yield of 51%. The result showed that the origin of the oxygen atom in the desired product was only from oxygen gas since no ^{16}O-labeled product was found. To investigate the reaction mechanism further, EPR measurements were performed with illumination from a laser source. The room temperature X-band EPR spectrum of PCN in ACN in air before illumination showed a broad singlet (R1) which grew upon illumination and was assigned as the radical signal of the photocatalyst (**Table 2**, **Figure 4** left). Illumination in the presence of Cl_4NHPI gave a second signal (R2), a triplet, which grew over the course of 210 s and was assigned to the Cl_4PINO radical. When cumene was also added, a strong R2 signal appeared immediately upon illumination which decayed over 210 s. In order to detect shorter living radical species, DMPO was introduced as a spin-trap. Illumination of PCN in ACN in air with DMPO gave a clear multiline signal (R3) with EPR parameters (**Table 2**, **Figure 4** right) consistent with those of the protonated spin-trapped adduct of $O_2^{\bullet-}$ (DMPO-OOH). Illumination in the presence of Cl_4NHPI gave an additional intense signal (R4), which

appeared to be a nitroxide radical, but did not resemble any known DMPO spin-trapped adduct. Since the R2 signal was not detected, we suspect that R4 is a byproduct of an unknown interaction between the Cl_4PINO radical and DMPO. Over 210 s of illumination, both R3 and R4 decayed. When cumene was also added a weak multiline spectrum was already observed before the illumination. Upon illumination strong signals for R3, R4 alone with a third species (R5) could observed. However, like the case without cumene, the signals for R3 and R4 decayed over the course of 210 s, leaving only R5 which has EPR parameters very similar to R3 suggesting that was also a DMPO-OOR adduct (**Table 2**).

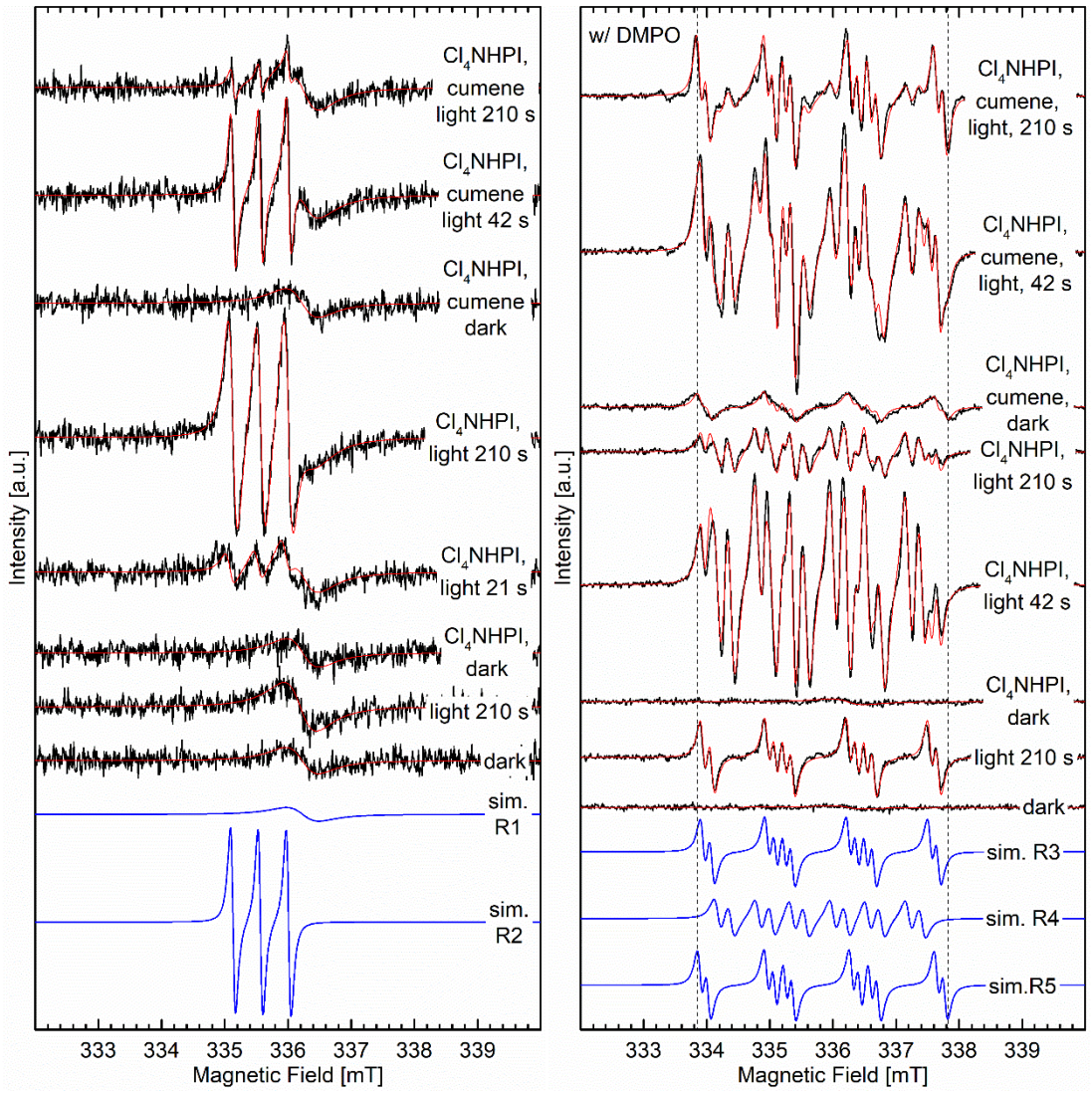

Figure 4. cw X-band (~9.44 GHz) EPR spectra of PCN catalyst (~ 1 mg) in ACN in air with (right) or without (left) DMPO (10 vol%), with and without Cl_4NHPI (60 uM), cumene (200 mM) or illumination (447 nm, ~200 mW) recorded at room temperature using 1 mW microwave power, 0.05 mT modulation amplitude and 100 kHz modulation frequency. The simulation of each spectra is shown in red and the different components used fro the simulation is shown in blue. The dash lines help guide the eye to the difference in line-spltting between R3 and R5.

Table 2: EPR simulation parameters of the radicals observed in this work in comparison to reported parameters. Hyperfine coupling *A* are given in mT.

Radical	solvent	$A_{N(iso)}$	$A_{H(iso)}$	g_{iso}	Ref.
R1	MeCN			2.0039	This work
R2	MeCN	0.52	-	2.0078	This work
R3	MeCN	1.29	1.02 (H_β), 0.13 (H_γ)	2.0063	This work
R4	MeCN	1.19	0.65 (H_β), 0.21 (H_γ)	2.0064	This work
R5	MeCN	1.35	1.06 (H_β), 0.13 (H_γ)	2.0062	This work
p-TFAB-C_3N_4	EtOH	-	-	2.0038	Ref. 24
g-C_3N_4		-	-	2.0034	Ref. 37
Cl_4NOPI radical	MeCN, 1 M py, 50 mM NBu_4PF_6	0.441	-	2.0074	Ref. 38
DMPO-$^{\bullet}$OOH	MeCN	1.326	1.061 (H_β), 0.140 (H_γ)	2.0061	Ref. 39
DMPO-$OOC(CH_3)_2Ph$	Toluene	1.392	1.12	-	Ref. 40
	Water pH 3	1.450	1.075 (H_β), 0.175 (H_γ)		Ref. 41
DMPO-$OC(CH_3)_2Ph$	Toluene	1.308	0.888 (H_β), 0.168(H_γ)	-	Ref. 40

Based on the EPR results and our previous investigations of photocatalytic reactions[42-44] as well as literature reports of the heterogeneous photocatalysis and HAT process,[45,46] we suggested the following mechanism (**Scheme 4)**. In the first step, the catalyst is activated under the irradiation of blue LED (or laser) and positive holes (h^+) and electrons (e^-) are generated on the surface of the catalyst. As demonstrated by the detection of the DMPO-OOH adduct, O_2 is reduced through SET by the conduction band of the catalyst forming the superoxide radical anion ($O_2^{\bullet-}$).[47] The Cl_4PINO radical (directly detected by EPR) is subsequently generated through HAT process with $O_2^{\bullet-}$, while $O_2^{\bullet-}$ is reduced to HOO^-. Afterwards, HOO^- undergoes oxidation by the VB of the photocatalyst and another hydrogen atom from a second HAT to form hydrogen peroxide. Meanwhile, another Cl_4PINO radical is activated through this process. The buildup of the Cl_4PINO radical signal (R2) over the illumination time in the absence of the substrate are consisted with these proposed pathways. In the second step, the substrate was

activated by the Cl_4PINO radical through another HAT process and to form the substrate radical (**1c**) at the benzylic site. The decrease of the Cl_4PINO radical signal (R2) over the illumination time in the presence of the substrate are consistent with this step. Subsequently, the substrate radical reacted with oxygen and formed the intermediate **1d**. The detection of a second possible DMPO-OOR adduct (R5) which predominates at the end of the illumination period fits with this proposal. Indeed, the EPR parameters for R5 are similar to those reported for DMPO trapped **1d** in different solvents (**Table 2**). Finally, a H atom is abstracted from Cl_4NHPI via HAT to form **1e**, and product **1b** is generated by eliminating O_2.

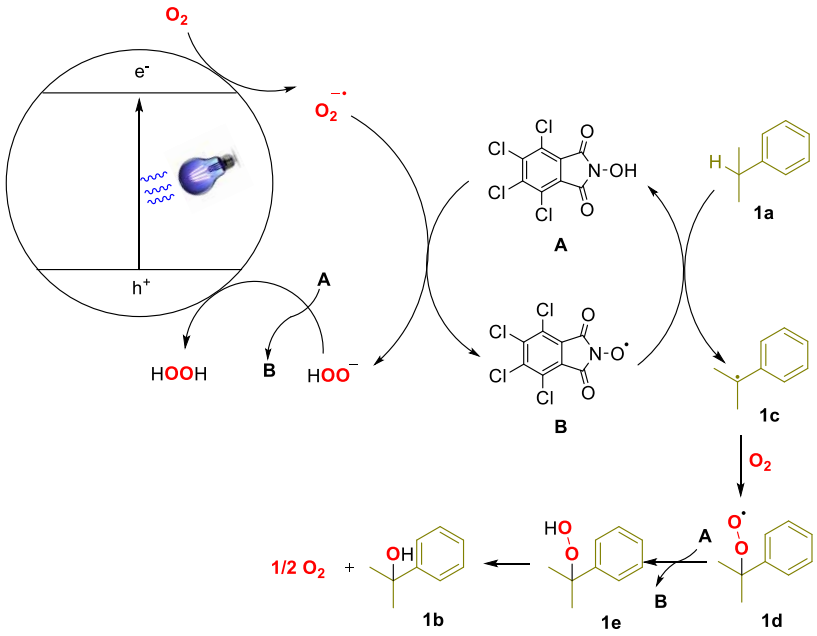

Scheme 4. Suggested mechanism of photocatalytic hydroxylation.

CONCLUSION

In summary, a semi-heterogeneous metal-free catalytic system based on PCN/Cl_4NHPI has been developed for the selective hydroxylations at the tertiary benzylic C-H bonds using oxygen as the oxidant as well as the oxygen source. Versatile benzylic substrates were employed under these mild reaction conditions to afford desirable tertiary alcohols in moderate to excellent isolated yields. More importantly, the *g*-scale reaction was achieved by using cleaner and greener energy source, sunlight in this reaction. The stability of the catalyst was proved *via* recycling the catalyst at least five-times and detailed spectroscopic analyses. The EPR measurement was also carried out to provide the possible mechanism. Structure determination based on solid state NMR spectroscopy, including ^{1}H MAS NMR, ^{1}H- ^{13}C, and ^{1}H- ^{15}N CPMAS (c) spectra of PCN, allowed to derive an understanding of the photocatalytic activity at the atomic level. In particular, both the linkers (NH) and terminal NH_2 that built about the extended C_3N_4 network was confirmed at natural abundance without the application of expensive ^{15}N labelling. The NMR results indicated that the structure of PCN was not characterized by a significantly high number of defects originating from nitrogen-deficiency in the structure. This indicated that the role of the defect concentration for C_3N_4-based materials could have been previously overestimated when elucidating the reaction mechanism in photocatalytic reactions.

AUTHOR INFORMATION

Corresponding Author

Shoubhik Das - Department of Chemistry, University of Antwerp, Groenenborgerlaan 171, 2020 Antwerpen, Belgium, Email: shoubhik.das@uantwerpen.be

Authors

Yu Zhang−Institut für Organische und Biomolekulare Chemie, Georg-August-Universität Göttingen, Tammannstraße 2, 37077 Göttingen, Germany; Department of Chemistry, University of Antwerp, Groenenborgerlaan 171, 2020 Antwerpen, Belgium.

Shaowei Qin−Institut für Organische und Biomolekulare Chemie, Georg-August-Universität Göttingen, Tammannstraße 2, 37077 Göttingen, Germany.

Nathalie Claes−EMAT, University of Antwerp, Groenenborgerlaan 171, 2020 Antwerp, Belgium.

Waldemar Schilling−Institut für Organische und Biomolekulare Chemie, Georg-August-Universität Göttingen, Tammannstraße 2, 37077 Göttingen, Germany.

Prakash Kumar Sahoo−ORSY Division, Department of Chemistry, Universiteit Antwerpen, Campus Groenenborger, Groenenborgerlaan 171, 2020 Antwerpen, Belgium.

H. Y. Vincent Ching−ORSY Division, Department of Chemistry, Universiteit Antwerpen, Campus Groenenborger, Groenenborgerlaan 171, 2020 Antwerpen, Belgium.

Aleksander Jarowski−Department of Materials and Environmental Chemistry, Stockholm University, 10691 Stockholm, Sweden.

Adam Slabon−Department of Materials and Environmental Chemistry, Stockholm University, 10691 Stockholm, Sweden.

Filip Lamiere−BAMS, Department of Chemistry, University of Antwerp, Groenenborgerlaan 171, 2020 Antwerp, Belgium.

Sabine van Doorslaer−IMEF, Department of Chemistry, University of Antwerp, Universiteitsplein 1, 2610 Antwerp, Belgium.

Sara Bals−EMAT, University of Antwerp, Groenenborgerlaan 171, 2020 Antwerp, Belgium.

Author Contributions

†Y.Z. and S. Q. contributed equally.

Acknowledgement

We thank BOF joint PhD grant (to Y. Z.), Francqui Foundation and FWO research grant (to S.D.), Chinese Scholarship Council (to Y.Z.). A.S. would like to thank the Swedish Energy Agency for financial support (project nr: 5050-1). The SEM microscope was partly funded by the Hercules Fund from the Flemish Government.

REFERENCE

1. Khan, I. A.; Abourashed, E.A., Leung's encyclopedia of common natural ingredients: used in food, drugs and cosmetics. John Wiley & Sons. 2011.
2. Reed, N. L.; Yoon, T. P. (2021). Oxidase reactions in photoredox catalysis. *Chem. Soc. Rev.* **2021**, ***50***, 2954–2967.
3. Zhang, Y.; Schilling, W.; Das, S. Metal-Free Photocatalysts for C−H Bond Oxygenation Reactions with Oxygen as the Oxidant. *ChemSusChem* **2019**, *12*, 2898–2910.
4. Hochgürtel, M.; Ralf B.; Heiko K.; Dorothea P.; Michael W. H.; Sonja K.; Otmar S.; Claude N.; Alexey V. E. Ketones as building blocks for dynamic combinatorial libraries: highly active neuraminidase inhibitors generated via selection pressure of the biological target. *J. Med. Chem.* **2003**, *46*, 356–358.

5. Lessa, J. A.; Isolda C. M.; Paulo RO da S.; Marcella A. S.; Raquel G. dos S.; Nivaldo L. S.; Nelilma C. R.; Eliezer J. B.; Heloisa B, 2-Acetylpyridine thiosemicarbazones: cytotoxic activity in nanomolar doses against malignant gliomas. *Eur. J. Med. Chem.* **2010**, *45*, 3904–3910.
6. Chambers, R. K., Zhao, J., Delaney, C. P., & White, M. C. Chemoselective Tertiary C− H Hydroxylation for Late-Stage Functionalization with Mn (PDP)/Chloroacetic Acid Catalysis. *Adv. Synth. Catal.* **2020***, 362*, 417−423.
7. Bigi, M. A., Reed, S. A., White, M. C. Diverting non-haem iron catalysed aliphatic C–H hydroxylations towards desaturations. *Nature Chem.*, **2011**, *3*, 216.
8. Gormisky, P. E.; White, M. C. Catalyst-controlled aliphatic C–H oxidations with a predictive model for site-selectivity. *J. Am. Chem. Soc.* **2013**, *135*, 14052−14055
9. Kawamata, Y.; Yan, M.; Liu, Z.; Bao, D. H.; Chen, J.; Starr, J. T.; Baran, P. S. Scalable, electrochemical oxidation of unactivated C–H bonds. *J. Am. Chem. Soc.* **2017**, *139*, 7448-7451;
10. Sterckx, H.; Morel, B.; Maes, B. U. Catalytic aerobic oxidation of C (sp^3)−H bonds. *Angew. Chem. Int. Ed.* **2019**, *58*, 7946−7970.
11. Fukuda, O., Sakaguchi, S., & Ishii, Y. Preparation of Hydroperoxides by N-Hydroxyphthalimide-Catalyzed Aerobic Oxidation of Alkylbenzenes and Hydroaromatic Compounds and Its Application. *Adv. Synth. Catal*. **2001**, *343*, 809−813.
12. Zhang, L., Jie, S., Liu, Z. Bicontinuous mesoporous Co, N co-doped carbon catalysts with high catalytic performance for ethylbenzene oxidation. *New J. Chem*. **2019**, *43*, 7275−7281.
13. Liu, W., Zhang, L., Liu, X., Liu, X., Yang, X., Miao, S., Wang, W., Wang A., Zhang, T. Discriminating catalytically active FeN x species of atomically dispersed Fe–N–C catalyst for selective oxidation of the C–H bond. *J. Am. Chem. Soc.* **2017***, 139*. 10790-10798.
14. Noureldin, N. A., Zhao, D., Lee, D. G. Heterogeneous permanganate oxidations. 7. The oxidation of aliphatic side chains. *J. Org. Chem.* **1997**, *62*, 8767-8772.
15. Chandra, B., Singh, K. K., Gupta, S. S. Selective photocatalytic hydroxylation and epoxidation reactions by an iron complex using water as the oxygen source. *Chem. Sci.* **2017**, *8*, 7545-7551.
16. Lykakis, I. N.; Orfanopoulos, M. Photooxidation of aryl alkanes by a decatungstate/triethylsilane system in the presence of molecular oxygen. *Tetrahedron Lett.* **2004**, *45*, 7645;
17. Li, G.-X.; Morales-Rivera, C.A.; Gao, F.; Wang, Y.; He, G.; Liu, P.; Chen, G. A unified photoredox-catalysis strategy for C(sp^3)–H hydroxylation and amidation using hypervalent iodine. *Chem. Sci.* **2017**, *8*, 7180–7185.
18. Tanwar, L.; Börgel, J.; Ritter, T. Synthesis of Benzylic Alcohols by C−H Oxidation. *J. Am. Chem. Soc.* **2019**, *141*, 17983–17988.
19. Lesieur, M.; Battilocchio, C.; Labes, R.; Jacq, J.; Genicot, C.; Ley, S.; Pasau, P. Direct Oxidation of Csp^3-H bonds using in Situ Generated Trifluoromethylated Dioxirane in Flow. *Chem. Eur. J*. **2019**, *25*, 1203−1207.
20. Cauwenbergh, R., Das**,** S., Photocatalysis: A Green Tool for Redox Reactions, *Synlett*. **2021**, *32*, DOI: 10.1055/s-0040-1706042.
21. Cauwenbergh, R., Das, S., Photochemical reduction of carbon dioxide to formic acid. *Green Chem.* **2021**, *23*, 2553−2574.
22. Zhang, Y., Schilling, W., Das, S., Metal-Free Photocatalysts for C−H Bond Oxygenation Reactions with Oxygen as the Oxidant, *ChemSusChem* **2019**, *12*, 2898−2910.

23. Schilling, W., Zhang, Y., Riemer, D., Das, S., Visible-Light-Mediated Dearomatisation of Indoles and Pyrroles to Pharmaceuticals and Pesticides. *Chem. Eur. J.* **2020**, *26*, 390–395.
24. T. Zhang, W. Schilling, S. U. Khan, H. Y. V. Ching, C. Lu, J. Chen, A. Jaworski, G. Barcaro, S. Monti, K. De Wael, A. Slabon**,** S. Das, Atomic Level Understanding for the Enhanced Generation of Hydrogen Peroxide by Aryl Amino Polymeric Carbon Nitrides. *ACS Catal.* **2021**.
25. Savateev, A.; Antonietti, M. Heterogeneous organocatalysis for photoredox chemistry. *ACS Catal*. **2018**, *8*, 9790-9808.
26. Zheng, Y.; Lin, L.; Wang, B.; Wang, X. Graphitic carbon nitride polymers toward sustainable photoredox catalysis. *Angew. Chem. Int. Ed.* **2015**, *54*, 12868–12884.
27. Fechler, N., Zussblatt, N. P., Rothe, R., Schlögl, R., Willinger, M. G., Chmelka, B. F., Antonietti, M. Eutectic syntheses of graphitic carbon with high pyrazinic nitrogen content. *Adv. Mater.* **2016**, *28*, 1287–1294.
28. Zimmerman, J. B., Anastas, P. T., Erythropel, H. C., Leitner, W. Designing for a green chemistry future. *Science* **2020**, *367*, 397–400.
29. Wang, X., Maeda, K., Thomas, A., Takanabe, K., Xin, G., Carlsson, J. M., Domen, K., Antonietti, M. A metal-free polymeric photocatalyst for hydrogen production from water under visible light. *Nat. Mater.* **2009**, *8*, 76–80.
30. Wang, Y., Wang, X., Antonietti, M. Polymeric graphitic carbon nitride as a heterogeneous organocatalyst: from photochemistry to multipurpose catalysis to sustainable chemistry. *Angew. Chem. Int. Ed.* **2012**, *51*, 68–89.
31. Das, S., Murugesan, K., Villegas Rodríguez, G. J., Kaur, J., Barham, J. P., Savateev, A., Antonietti, M., König, B. Photocatalytic (het) arylation of C (sp^3)–H bonds with carbon nitride. *ACS Catal.* **2021**, *11*, 1593-1603.
32. Xu, C. Q.; Zhang, W. D. Facile synthesis of nitrogen deficient g-C_3N_4 by copolymerization of urea and formamide for efficient photocatalytic hydrogen evolution. *Mol. Catal.* **2018**, *453*, 85–92.
33. Szewczyk, I., Rokicinska, A., Michalik, M., Chen, J., Jaworski, A., Aleksis, R., Pell, A. J., Slabon, A., Kuśtrowski, P. Electrochemical Denitrification and Oxidative Dehydrogenation of Ethylbenzene over N-doped Mesoporous Carbon: Atomic Level Understanding of Catalytic Activity by ^{15}N NMR Spectroscopy. *Chem. Mater.* **2020**, *32*, 7263–7273.
34. Kushch, O.; Hordieieva, I.; Novikova, K.; Litvinov, Y.; Kompanets, M.; Shendrik, A.; Opeida, I. Kinetics of *N*-oxyl Radicals' Decay. *J. Org. Chem.* **2020**, *85*, 7112–7124.
35. Hu, Y., Shim, Y., Oh, J., Park, S., Park, S., Ishii, Y. Synthesis of ^{13}C-, ^{15}N-labeled graphitic carbon nitrides and NMR-based evidence of hydrogen-bonding assisted two-dimensional assembly. *Chem. Mater.* **2017**, *29*, 5080–5089.
36. Sehnert, J., Baerwinkel, K., Senker, J. Ab initio calculation of solid-state NMR spectra for different triazine and heptazine based structure proposals of g-C_3N_4. *J. Phys. Chem. B*, **2007**, *111*, 10671–10680.
37. Zhang, J., Zhang, G., Chen, X., Lin, S., Möhlmann, L., Dołęga, G., Lipner, G., Antonietti, M., Blechert, S., Wang, X. Co-monomer control of carbon nitride semiconductors to optimize hydrogen evolution with visible light. *Angew. Chem. Int. Ed.* **2012**, *51*, 3183–3187.
38. Buckingham, M. A., Cunningham, W., Bull, S. D., Buchard, A., Folli, A., Murphy, D. M., Marken, F. Electrochemically driven C−H hydrogen abstraction processes with the tetrachloro-phthalimido-N-oxyl (Cl_4PINO) catalyst. *Electroanalysis* **2018**, *30*, 1706–1713.

39. Ozawa, T., Hanaki, A. Hydroxyl radical produced by the reaction of superoxide ion with hydrogen peroxide: electron spin resonance detection by spin trapping. *Chem. Pharm. Bull.* **1978**, *26*, 2572–2575.
40. Rosen, G. M., Rauckman, E. J. Spin trapping of the primary radical involved in the activation of the carcinogen N-hydroxy-2-acetylaminofluorene by cumene hydroperoxide-hematin. *Mol. Pharmacol.* **1980**, *17*, 233–238.
41. Davies, M. J., Slater, T. F. Studies on the photolytic breakdown of hydroperoxides and peroxidized fatty acids by using electron spin resonance spectroscopy. Spin trapping of alkoxyl and peroxyl radicals in organic solvents. *Biochem. J.* **1986**, *240*, 789–795.
42. Schilling, W., Zhang, Y., Sahoo, P. K., Sarkar, S. K., Gandhi, S., Roesky, H. W., Das, S. Nature inspired singlet oxygen generation to access α-amino carbonyl compounds via 1, 2-acyl migration. *Green Chem.* **2021**, *23*, 379–387.
43. Schilling, W.; Riemer, D.; Zhang, Y.; Hatami, N.; Das, S. Metal-free catalyst for visible-light-induced oxidation of unactivated alcohols using air/oxygen as an oxidant. *ACS Catal.* **2018**, *8*, 5425–5430.
44. Zhang, Y.; Schilling, W.; Riemer, D.; Das, S. Metal-free photocatalysts for the oxidation of non-activated alcohols and the oxygenation of tertiary amines performed in air or oxygen. *Nat. Protoc.* **2020**, *15*, 822–839.
45. Wang, Y.; Chen, X.; Jin, H.; Wang, Y. Mild and Practical Dirhodium (II)/NHPI-Mediated Allylic and Benzylic Oxidations with Air as the Oxidant. *Chem. Eur. J.* **2019**, *25*, 14273–14277.
46. Liu, G.; Tang, R.; Wang, Z. Metal-free allylic oxidation with molecular oxygen catalyzed by g-C_3N_4 and *N*-hydroxyphthalimide. *Catal. Lett.* **2014**, *144*, 717–722.
47. Zhang, Y.; Hatami, N.; Lange, N. S.; Ronge, E.; Schilling, W.; Jooss, C.; Das, S. A metal-free heterogeneous photocatalyst for the selective oxidative cleavage of C=C bonds in aryl olefins via harvesting direct solar energy. *Green Chem.* **2020**, *22*, 4516–4522.